Seasonal cycle of volume transport through Kerama Gap revealed by a 20-year global HYbrid Coordinate Ocean Model reanalysis

Zhitao Yu [a,b,*], E. Joseph Metzger [b], Prasad Thoppil [b], Harley E. Hurlburt [c], Luis Zamudio [c], Ole Martin Smedstad [d], Hanna Na [e], Hirohiko Nakamura [f], Jae-Hun Park [g]

[a] American Society of Engineering Education, DC, USA
[b] Naval Research Laboratory, Stennis Space Center, MS, USA
[c] Florida State University, Tallahassee, FL, USA
[d] Vencore, Incorporated, Stennis Space Center, MS, USA
[e] Faculty of Science, Hokkaido University, Sapporo, Japan
[f] Faculty of Fisheries, Kagoshima University, Kagoshima, Japan
[g] Department of Ocean Sciences, Inha University, Incheon, South Korea

ARTICLE INFO

ABSTRACT

The temporal variability of volume transport from the North Pacific Ocean to the East China Sea (ECS) through Kerama Gap (between Okinawa Island and Miyakojima Island − a part of Ryukyu Islands Arc) is investigated using a 20-year global HYbrid Coordinate Ocean Model (HYCOM) reanalysis with the Navy Coupled Ocean Data Assimilation from 1993 to 2012. The HYCOM mean transport is 2.1 Sv (positive into the ECS, 1 Sv = 10^6 m³/s) from June 2009 to June 2011, in good agreement with the observed 2.0 Sv transport during the same period. This is similar to the 20-year mean Kerama Gap transport of 1.95 ± 4.0 Sv. The 20-year monthly mean volume transport (transport seasonal cycle) is maximum in October (3.0 Sv) and minimum in November (0.5 Sv). The annual variation component (345–400 days), mesoscale eddy component (70–345 days), and Kuroshio meander component ($<$ 70 days) are separated to determine their contributions to the transport seasonal cycle. The annual variation component has a close relation with the local wind field and increases (decreases) transport into the ECS through Kerama Gap in summer (winter). Most of the variations in the transport seasonal cycle come from the mesoscale eddy component. The impinging mesoscale eddies increase the transport into the ECS during January, February, May, and October, and decrease it in March, April, November, and December, but have little effect in summer (June–September). The Kuroshio meander components cause smaller transport variations in summer than in winter.

© 2015 Elsevier Ltd. All rights reserved.

1. Introduction

The Kuroshio is one of the world's major western boundary currents and a key feature of North Pacific Ocean circulation. It originates from the North Equatorial Current (Gordon et al., 2014) and then enters the East China Sea (ECS) through the East Taiwan Channel (ETC) between Taiwan and Ishigaki Island; it carries warm and saline waters poleward (Oka and Kawabe, 1998), and exits the ECS through Tokara Strait (Fig. 1). Estimates of the mean Kuroshio transport in the ECS vary from 18.5 to 32 Sv (Roemmich and McCallister, 1989; Johns et al., 2001; Andres et al., 2008b). Because the Kuroshio transports significant amounts of heat, salt, and mass from the tropical ocean to mid-latitudes, it has a great influence on the global climate and

heat balances (Qu and Lukas, 2003), and on the fisheries, hydrography, and weather of countries surrounding the Northwestern Pacific (Qiu, 2001).

The Ryukyu Islands Arc forms a barrier along the eastern side of the ECS and separates the ECS from the North Pacific except at connecting straits. Thus, except at the entrance (ETC) and exit (Tokara Strait), the water in the ECS and the North Pacific exchanges through many channels in the Ryukyu Islands Arc. Kerama Gap, located between Miyakojima and Okinawa (Fig. 1), is the deepest channel with a sill depth of 1050 m (Choi et al., 2002) and thus has been the subject of significant research. Analyzing moored current meter (CM) observations, Yuan et al. (1994) reported an observed 5.8 Sv outflow (from the ECS to the Northwestern Pacific) through the passages between Miyakojima and Okinawa during Fall 1991; but Yuan et al. (1995) estimated a 2.4 Sv inflow (from the Northwestern Pacific into the ECS) from November 1991 to September 1992. Morinaga et al. (1998) estimated a 7.2 Sv inflow through Kerama Gap from their CM
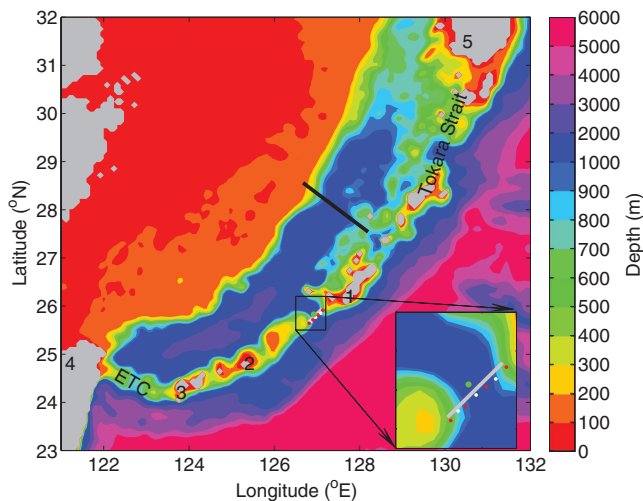
Fig. 1. HYCOM bathymetry (meters) for the East China Sea. Gray represents model land points. Okinawa (1), Miyakojima (2), Ishigaki (3), the East Taiwan Channel (ETC), Taiwan (4), Kyushu (5), and Tokara Strait are labeled. The black line represents the PN-line. The land -ocean boundary in HYCOM is defined by the 10 cm isobath but all depths less than 5 m are set to 5 m. A zoom centered on Kerama Gap is inset in the lower right corner. The gray solid line represents the HYCOM transect used to determine transport through Kerama Gap. The four red dots represent the locations of CPIES moorings ES1 to ES4 and three white dots represent the locations of current meters CM1 to CM3 (SW-NE, Na et al., 2014). The green dot represents the location of CPIES mooring ES5. (For interpretation of the references to color in this figure legend, the reader is referred to the web version of this article).

observations during two months from July to September 1992. The wide range of observed transports can be attributed to the relatively short observation duration periods covering different observation times and is indicative of the large temporal variations in transport through Kerama Gap. The annual mean transport through Kerama Gap remained uncertain until Na et al. (2014) reported a 2.0 Sv mean flow into the ECS based on two years of observations covering June 2009–June 2011. The standard deviation is 3.2 Sv, which is much larger than the 2-year mean inflow and comparable to the standard deviation of the downstream PN-line (Fig. 1, black line) Kuroshio transport (4.0 Sv) (Andres et al., 2008b). Hence, Kerama Gap transport may have a significant impact on the temporal variability of the Kuroshio transport in the ECS.

Classical theories have shown that mid-latitude eastward flows have a spontaneous tendency to develop wavelike disturbances due to baroclinic instability (Kundu and Cohen, 2002). Since the Kuroshio Extension and the Subtropical Countercurrent both exist at mid-latitudes, there is no surprise that mesoscale eddies are ubiquitous outside of the ECS with the Ryukyu Islands Arc acting as a barrier. Andres et al. (2008a, b) show that the eddies arriving from the ocean interior affect the transport through Kerama Gap and then the Kuroshio transport in the ECS. Andres and Cenedese (2013) further found laboratory support for Andres et al. (2008a, b). Jin et al. (2010), on the other hand, argued that a shifting of the Kuroshio mean current axis and the approaching eddies are both important in determining flow direction through Kerama Gap. The preceding results indicate the important role of the Kerama Gap in the interaction of the ECS-Kuroshio with the ocean interior and on water exchange through the Ryukyu Islands Arc.

In a numerical attempt to simulate Ryukyu currents with climatological forcing, You and Yoon (2004) reported a 5.6 Sv inflow through the passages between Miyakojima and Okinawa. In their model, spatial resolution is 1/6°. Guo et al. (2006) ran a 1/18° nested ocean model using weekly forcing over the period from September 1991 to December 1998 and found an inflow of 0.49 Sv between Miyakojima and Okinawa. Soeyanto et al. (2014) estimated a 0.18 Sv inflow

through Kerama Gap by analyzing the results from a 20-year (1993–2012) reanalysis output by a data-assimilative ocean model, which is based on the Princeton Ocean Model with a generalized coordinate system, developed in Japan Coastal Ocean Predictability Experiments 2. Their model includes two sub-models that are connected by a one-way nesting system and the horizontal grid interval for the inner model (10.5–60°N, 108–180°E) is 1/12°. All of these numerical studies reported inflow through Kerama Gap, which is consistent with Na et al. (2014), yet the mean transport is quite different. Kerama Gap has very steep topography and its width is only about 50 km. Thus, resolving the transport requires fine horizontal resolution and a vertical coordinate system capable of resolving the vertical structure of flow from the surface to the sill depth. Additionally, data assimilation of sea surface height (SSH) is necessary for the model to capture the temporal transport variation generated by approaching eddies.

Na et al. (2014) have investigated the dynamics at Kerama Gap and reported the mean transport. To elucidate the dynamics underlying the variation of transport through Kerama Gap, it is necessary to estimate its variability at various timescales. However, the 2-year observational period is not long enough to determine variability in timescales longer than one year. In this study, we present a 20-year (1993–2012) transport time series through Kerama Gap from a data assimilative global HYbrid Coordinate Ocean Model (HYCOM) reanalysis. The long transport time series provides a unique opportunity that allows us to define the seasonal cycle and to investigate the impact of transport variability at different time scales on the seasonal cycle. Previous studies (Sugimoto et al., 1988; Qiu et al., 1990; James et al., 1999; Ichikawa, 2001; Nakamura et al., 2003) also show that two types of Kuroshio meanders exist in the northern Okinawa trough with periods less than 70 days. Thus, we focus on three bands with periods of 345–400 days (annual variation), 70–345 days (mesoscale eddy), and shorter than 70 days (Kuroshio meander) and also examine their respective contributions to the seasonal cycle. The paper is organized as follows: the numerical model used in this study is described in Section 2. Model comparisons with observational data are presented in Section 3. Transport variability is described in Section 4. Dynamics underlying the transport variability are discussed in Section 5, followed by conclusions in Section 6.

2. Numerical model

HYCOM is a primitive equation general ocean circulation model applied to large scale, marginal sea, and coastal studies. A detailed description of HYCOM physics can be found in Bleck (2002). Below, HYCOM is briefly presented with emphasis on the model aspects that are relevant for this study.

HYCOM solves five prognostic equations: two for horizontal velocity components, a mass continuity equation, and two conservative equations that govern temperature and salinity. The prognostic equations are time-integrated using a split-explicit treatment of barotropic and baroclinic modes. There are three vertical-coordinate systems coexisting in HYCOM: z-coordinates in unstratified water, sigma-coordinates in shallow depths, and isopycnal coordinates in the stratified ocean. Hence, HYCOM maintains the significant advantages of an isopycnal model in the stratified ocean, but allows coordinate surfaces to locally deviate from isopycnals to provide more vertical resolution near the surface and in shallow coastal regions in order to better represent the upper ocean physics (Chassignet et al., 2003). With this unique feature, HYCOM serves as a good tool for simulating circulations near Kerama Gap, which has complex topography that covers the shallow water near Kerama Gap and Okinawa Island, the Okinawa trough, slope, and the deep ocean.

The data assimilation scheme employed for the reanalysis is a three dimensional variational scheme (3DVAR) used within the Navy Coupled Ocean Data Assimilation (NCODA) (Cummings, 2005; Cummings and Smedstad, 2013). The ocean data sets assimilated by

NCODA include: remotely sensed sea surface temperature (SST), SSH, and sea ice concentration; plus in-situ surface and subsurface observations of temperature and salinity. An important component within NCODA is forming 3D synthetic profiles from the 2D SSH and SST, since there are only very limited subsurface profile data to constrain the system. In the global HYCOM reanalysis, HYCOM assimilates synthetic temperature profiles computed using the Modular Ocean Data Assimilation System (MODAS), which models the time-averaged co-variability of SSH and subsurface temperature at a given location (Fox et al., 2002). Salinity is then estimated from the synthetic temperature profiles using temperature-salinity regression relationships derived from the historical profiles archived in the MODAS database.

Global HYCOM is eddy resolving with an equatorial horizontal resolution of 0.08° (1/12.5°). There are 32 hybrid vertical coordinate layers with potential density referenced to 2000 m, the same as the present operational US Navy Global Ocean Forecast System version 3.0 (Metzger et al., 2014). The surface wind and thermal forcing are the 0.3125° 1-hourly Climate Forecast System Reanalysis (CFSR) products provided by National Centers for Environmental Prediction (NCEP) (Saha et al., 2010). The ocean reanalysis was initialized from a non-assimilative global HYCOM simulation spun-up to statistical equilibrium using a climatology of NCEP CFSR forcing. The data assimilation began on October 1, 1992 and the mesoscale eddy field adjusted to the satellite altimeter data within the first month. We analyzed model output over the period January 1993 through December 2012.

3. Model comparisons with observational data

In this section, we compare HYCOM reanalysis results with observational results which were obtained by Na et al. (2014) during two years from June 2009 to June 2011 at an array of current and pressure-recording inverted echo sounders (CPIESs) and CM moorings. The cross-section, formed with four CPIESs (ES1 to ES4, red dots in Fig. 1) and three CMs (CM1-3, white dots in Fig. 1), is located between ES1 and ES4. The HYCOM transect starts from the grid point nearest to ES1 and ends at the grid point closest to ES4, forming a 45° angle with respect to due east (Fig. 1, gray line). To be consistent with observations, a 72-h low-pass filter was applied to the daily transport time series from the HYCOM reanalysis.

3.1. Current velocity in Kerama Gap

Three CMs mentioned above and deployed during the 2-year observational period are CM1 to CM3 (from southwest to northeast) with ~15 km spacing between each mooring. The HYCOM grid points closest to the location of the three CMs are chosen to represent the model location of the CMs. Velocity time series are extracted from the "model CM" locations, linearly interpolated to the CM depth, and then temporally averaged and compared with observations (Fig. 2). The average distance between the "model CM" and the deployed CM location is ~3 km, larger than one third of the grid interval. Given the very steep cross-channel bathymetry and a ~50 km channel width, it can be difficult to obtain a good point-to-point model-data comparison. Below we first compare the yearly averaged currents at each CM in different layers and then provide the correlation coefficient to determine the temporal agreements between the reanalysis and observed current time series. The 2-year observational period is not sufficiently long to discuss the annual variation component. So we only focus on the mesoscale eddy and the Kuroshio meander components for the 2-year observational period.

In the upper (Fig. 2a and b) and middle (Fig. 2c and d) layers of Kerama Gap, both the observations (black) and reanalysis (red) show the strongest mean currents at CM3 (the northeasternmost CM). Following Na et al. (2014) analysis, we divide the period into year-1 (June
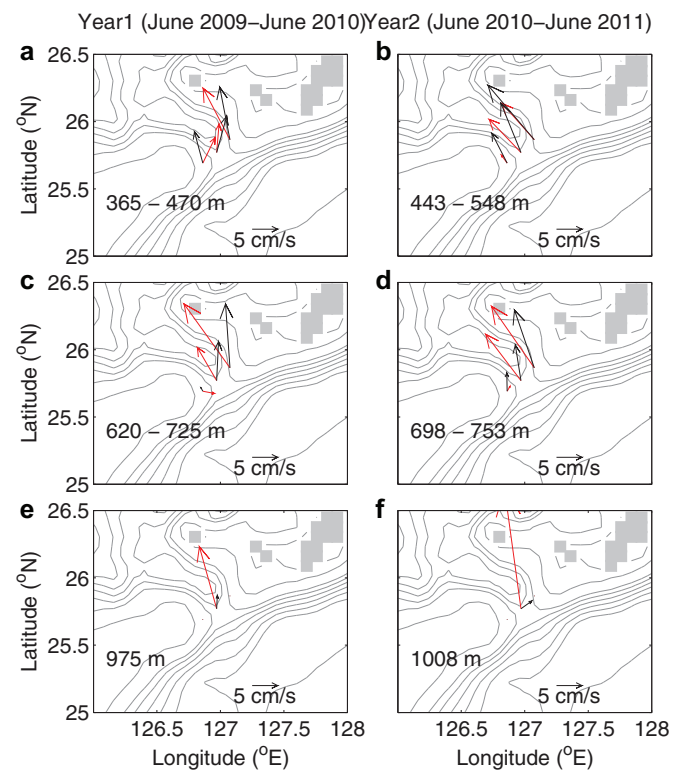

Fig. 2. Mean current vectors at upper (a, b), middle (c, d), and near sill depth (e, f) layers in Kerama Gap for year-1 (left) and year-2 (right) at CM1 (southwest) to CM3 (northeast). Only CM2 has measurements near the sill depth. Observations from Na et al. (2014) are shown in black and the HYCOM reanalysis in red. Gray represents model land points. The reference vector is shown in the lower right corner of each panel. (For interpretation of the references to color in this figure legend, the reader is referred to the web version of this article).

2009–June 2010) and year-2 (June 2010–June 2011). In both year-1 and year-2, the mean currents gradually decrease from northeast (CM3) toward the southwest (CM1) in Kerama Gap. The magnitude of the mean currents is reproduced better than the mean current direction. This discrepancy may be due to the topographic difference between reality and numerical model, as the current direction is more highly sensitive to the local topography compared with the current speed.

In the upper layer (Fig. 2a and b), the observations in year-1 show that mean currents at CM2 flow more normal to rather than parallel to the mean CM3 current direction. The HYCOM reanalysis correctly reproduces this characteristic. The year-2 reanalysis accurately reproduces the mean current direction in the upper layer for both CM1 and CM3.

In the middle layer (Fig. 2c and d), mean current directions in both the observations and HYCOM reanalysis are almost parallel to each other at CM2 and CM3 while the northwestward mean current direction in observations is not reproduced in the HYCOM reanalysis. At CM1, the HYCOM reanalysis mean current in year-1 shows weak outflow (2.3 cm/s) that is different from the observations showing even weaker inflow (0.7 cm/s). The HYCOM reanalysis mean current direction (into the ECS) is more consistent with the observations during year-2 than year-1 and the HYCOM reanalysis reproduces observations that the inflow at CM1 in year-2 is larger than in year-1.

The biggest discrepancy between the HYCOM reanalysis and current observations is in the deep layer (Fig. 2e and f), near the bottom. Though both the reanalysis and observations show mean inflow through Kerama Gap into ECS, the inflow magnitude (17.3 cm/s) of the reanalysis is much larger than observed (2.5 cm/s) at the center of Kerama Gap (CM2). The HYCOM reanalysis appears to have
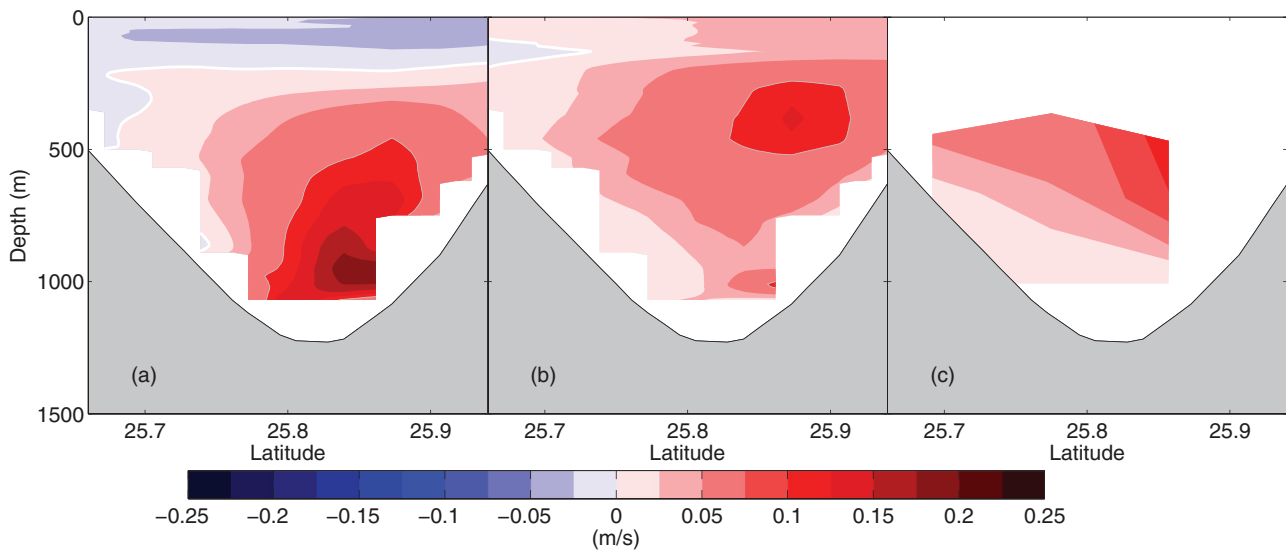
Fig. 3. Vertical structure of velocity (m/s) normal to the Kerama Gap transect for (a) the global HYCOM reanalysis, (b) Pacific assimilative HYCOM hindcast, and (c) linear interpolation of the observations (Na et al., 2014). The time frame spans the observational period, June 2009–June 2011.

bottom-trapped inflow at CM2 with the maximum occurring near the sill depth (Fig. 3a) while observations (Fig. 3c) do not show this feature. The cause of the excessive deep flow appears to be related to the use of MODAS synthetic profiles within NCODA that are used for projecting surface information downward into the water column. Cummings (2005) notes that MODAS has marginal skill in areas where profiles are limited, and the historical database seems inadequate to statistically represent the Ryukyu Current in the vicinity of Kerama Gap. A data-assimilative Pacific basin HYCOM hindcast spanning the Na et al. (2014) observational time period uses an improved methodology, Improved Synthetic Ocean Profiles (ISOP), for the downward projection of surface information (Helber et al., 2013) and shows better current structure agreement (Fig. 3b) with observations than the reanalysis, which supports the above explanation.

Nakamura et al. (2013) compared currents in the deep layer (black arrow in Fig. 2e and f) with currents observed by ES5 (location shown in Fig. 1, green dot) at a depth of 1366 m, 50 m above the sea floor, and suggested a thin vertical layer near the bottom with intensified inflow across Kerama Gap. Results from the data-assimilative Pacific HYCOM hindcast (Fig. 3b) agrees with this suggestion, though the currents in the bottom layer are not as strong as observed and the area with intensified bottom flow exists only on the northeastern sill.

Thoppil et al. (2015) compared the reanalysis results with 3.5 years of moored CM observations (Ryukyu currents) during December 1998 through October 2002 to the southeast of Amami-Ohshima Island (Ichikawa et al., 2004). Their comparison has shown good agreement at depths of 2000, 3000, and even below 4000 m (at these depths, the flow is not constrained by the data assimilation). Thus the mismatch of the bottom current through Kerama Gap should not be interpreted against the deep circulation of the reanalysis in general but rather confirms that MODAS has marginal skill in areas where profiles are limited.

The time series of the mesoscale eddy and Kuroshio meander components are calculated respectively by applying a band pass filter for periods of 70–345 days and a high pass filter for periods shorter than 70 days to the time series of total velocity component along Kerama Gap. The Fourier filter takes the Fourier transform of the time series, manipulates the specific frequency components, and finally inverse transforms the results. The correlation coefficients between reanalysis and observed along Kerama Gap velocity are summarized in Table 1 for the two different components. The correlation coefficients are all significant to the 95% confidence level calculated based

Table 1
Correlation coefficient between observed and modeled along Kerama Gap velocity at different CMs and layers during June 2009–June 2011 for the two period bands: mesoscale eddy (eddy, 70–345 days) and Kuroshio meander (meander, < 70 days) band. The correlation coefficients are all significant to the 95% confidence level.

	CM1		CM2		CM3	
	Eddy	Meander	Eddy	Meander	Eddy	Meander
Upper	0.66	0.22	0.62	0.29	0.67	0.26
Middle	0.39	0	0.68	0.23	0	0.37
Deep	N/A	N/A	0	0.19	N/A	N/A

on a student t distribution and 50–74 equivalent degrees of freedom (EDOF) for the eddy component and 402-654 EDOF for the Kuroshio meander component. It can be seen that the mesoscale eddy components are highly correlated and have a much higher positive correlation coefficient (greater than 0.62 in the upper layer) than the Kuroshio meander components (between 0.22 and 0.29 in the upper layer) in general except in the deep layer (CM2) and the middle layer of CM3. Mesoscale eddies are well integrated into the reanalysis through SSH data assimilation. The less significant correlation in the deep layer of CM2 and the middle layer of CM3 reflects that MODAS has marginal skill for projecting surface information downward into the water column in the northeast Kerama Gap.

3.2. Volume transport through Kerama Gap

Volume transport through a zonal (meridional) HYCOM transect is calculated as the product of the meridional (zonal) depth integrated barotropic velocity and the transect length. Volume transport through a diagonal HYCOM transect is estimated as a sum of the transport through the zonal and meridional transects, which starts from either end of the diagonal transect and ends at where the two transects intersect. Na et al. (2014) estimate that 60% of the mean transport is in the upper 500 m. The global HYCOM reanalysis indicates that 61% of the mean transport is in the upper 750 m (Fig. 3a), whereas the data-assimilative Pacific HYCOM hindcast indicates 65% of the mean transport is in the upper 500 m (Fig. 3b), a better agreement with the observations. This Pacific hindcast has a Kerama Gap mean transport of 2.05 Sv that also closely agrees with the observational estimate. Thus the mean inflow into the ECS does not
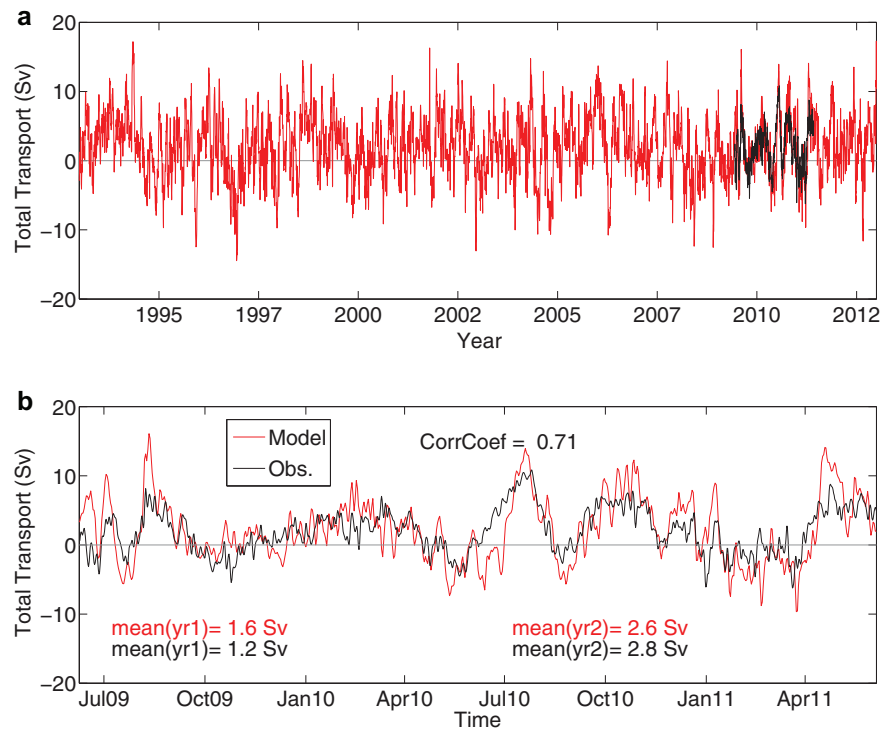
Fig. 4. Comparison of daily mean transport time series from the HYCOM reanalysis (red) with observations (black) from Na et al. (2014) through Kerama Gap. (a) The 20-year time series from 1993 to 2012, and (b) the 2-year observational period from June 2009 to June 2011. A 72-h low-pass filter has been applied to both time series. Positive transport is flow into the ECS and negative transport is flow into the Pacific through Kerama Gap. Mean values are listed in their respective colors. (For interpretation of the references to color in this figure legend, the reader is referred to the web version of this article).

Table 2
Statistics of transport (Sv) through the Kerama Gap. Year-1 is defined as the period from June 2009 to June 2010 and Year-2 is defined as June 2010–June 2011.

	2-year mean	Year-1 mean	Year-2 mean	2 year std	Year-1 std	Year-2 std
Observation	2.0	1.2	2.8	3.2	2.6	3.6
HYCOM	2.1	1.6	2.6	4.2	3.4	4.8

appear to be sensitive to the vertical structure of the currents and the conclusions drawn from the 20-year reanalysis are not impacted by the difference in the flow structure at the deep layer.

The HYCOM 20-year-long time series of volume transport through Kerama Gap is shown in Fig. 4a (red line). The time series during 2-year observation period is shown in Fig. 4b. The HYCOM reanalysis (red line in Fig. 4b) agrees well with observations (black line in Fig. 4b) but has slightly larger mean and variability. The mean total transport through Kerama Gap in the 2-year hindcast is 2.1 Sv (Table 2) into the ECS while the observation is 2.0 Sv, which is well within the standard error of estimate from the observations (0.7 Sv). The estimation error of the 2-year hindcast transport with respect to observed transport is ±0.4 Sv based on the auto-covariance function (Dewar and Bane, 1985) of the transport difference time series.

During the 2-year observational period, the HYCOM reanalysis captures the temporal transport variability well (Fig. 4b). The correlation coefficient between these two time series is 0.71, and this increases to 0.82 after applying a 20-day smoother to both time series. The correlation coefficient between the reanalysis and observation time series is 0.88 for the mesoscale eddy component, and 0.41 for the Kuroshio meander component.

Statistics for the two time series are shown in Table 2. The HYCOM reanalysis mean transports and standard deviations are all higher than the observed values except the mean transport for the second year. The HYCOM 2-year transport standard deviation is 4.2 Sv,

31% greater than the observed value. The HYCOM reanalysis shows that there is more flow into the ECS through Kerama Gap and more transport variation in year-2 (June 2010–June 2011) than in year-1 (June 2009–June 2010), in accord with the observations. The transport difference between year-1 and year-2 will be discussed further in Section 5.2.

4. Transport variability

The variance preserving power spectra of the 20-year-long transport time series is shown in Fig. 5. We divide the transport time series into four period bands: (1) inter-annual variation component with periods longer than 400 days, (2) annual variation component with periods between 345 and 400 days, (3) mesoscale eddy component with periods between 70 and 345 days, and (4) Kuroshio meander component with periods shorter than 70 days. Most of the variation comes from the mesoscale eddy and Kuroshio meander components, which explain 41.3% and 43.9% of the total variance, respectively. The inter-annual component accounts for 12.5% of the total variance, while the annual variation component contains only 2.3% of the total variance. In this section, we focus on the seasonal cycle of volume transport through Kerama Gap (Fig. 6), and examine how it is affected by each of the components mentioned above (Fig. 7, red, green, and blue lines) except the inter-annual variation component (Fig. 7, black dashed line).
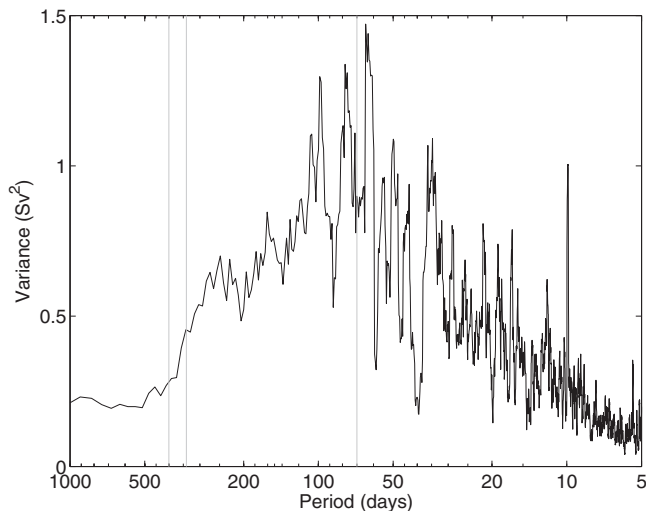
Fig. 5. Variance preserving power spectra ($S_v{}^2$) of the 20-year global HYCOM reanalysis transport time series through Kerama Gap. Vertical lines show the boundaries of the temporal bands investigated, i.e. 70, 345, and 400 days.
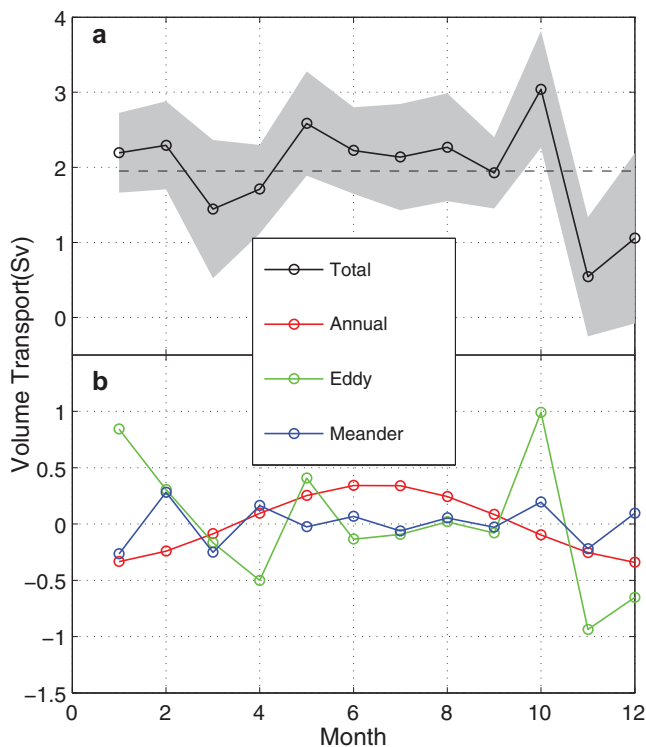

Fig. 6. (a) Seasonal cycle of transport through Kerama Gap and (b) the contribution of different signals to the transport seasonal cycle from the 1/12.5° global HYCOM reanalysis. The shaded area in (a) represents the seasonal cycle uncertainty and the dashed line shows the 20-year mean transport. (For interpretation of the references to color in this figure, the reader is referred to the web version of this article).

4.1. Mean transport and seasonal cycle

The HYCOM 20-year mean transport through Kerama Gap is 1.95 Sv into the ECS, with a standard deviation of 4.0 Sv. The uncertainty estimation of the 20-year mean transport is ± 0.28 Sv. Thus the 1.95 Sv mean is statistically significant.

By averaging the total transport month-by-month over the 20-year period, we obtain the 20-year mean seasonal cycle of transport through Kerama Gap (Fig. 6a, black solid line) and the associated uncertainty (Fig. 6a, shaded area). The most statistically significant

feature of the seasonal cycle is that the maximum transport occurs in October (3.04 Sv) followed by the minimum transport in November (0.54 Sv).

4.2. Annual variation component

We obtain the annual variation component (Fig. 7, red) by applying a band pass Fourier filter for periods of 345-400 days to the total transport time series. Explaining only 2.3% of the total variance, the amplitude of the annual variation component is as large as 2.0 Sv in 1997 and as small as 0.3 Sv in 2002. The standard deviation is 0.77 Sv. The 20-year monthly mean of the annual variation component indicates a clear cycle through Kerama Gap: inflow (0.34 Sv) into the ECS in summer and outflow (-0.34 Sv) from the ECS in winter (Fig. 6b, red line). The total transport inflow (Fig. 6a, black line) in summer is dominated by the annual variation component (Fig. 6b, red line).

4.3. Mesoscale eddy component

Previous studies (Feng et al., 2000; Zhang et al., 2001; Hsin et al., 2008; Lee et al., 2013) have attributed the long-term intra-annual (periods longer than 70 days) Kuroshio transport variability to interior Pacific mesoscale eddies. Similarly, Na et al. (2014) reported that the impinging mesoscale eddies from the interior Pacific Ocean are responsible for the long-term intra-annual variability through Kerama Gap. Thus we apply a band pass Fourier filter for periods of 70–345 days to the total transport time series and name the filtered time series the mesoscale eddy component (Fig. 7, green). This component has a standard deviation of 2.90 Sv.

The 20-year monthly mean of the mesoscale eddy component (Fig. 6b, green line) follows the seasonal cycle closely (Fig. 6a, black solid line). Its contribution to the seasonal cycle can be divided into three different stages: (1) neutral stage with a small magnitude from June through September, (2) an inflow stage in January, February, May, and October, and (3) an outflow stage in March, April, November, and December. The maximum occurs in October with 1.0 Sv of inflow and the minimum occurs in November with 0.9 Sv of outflow.

4.4. Kuroshio meander component

The short-term intra-annual (periods shorter than 70 days) Kuroshio fluctuations have been attributed to two types of Kuroshio meanders: (1) variations of the Kuroshio path meander with periods between 30 and 70 days (Ichikawa, 2001; Zhang et al., 2001; Nakamura et al., 2003), and (2) variations of the Kuroshio subsurface temperature frontal meander with periods shorter than 30 days (Sugimoto et al., 1988; Qiu et al., 1990; James et al., 1999; Feng et al., 2000). In this study, we apply a high pass Fourier filter for periods shorter than 70 days to the total transport time series to obtain the Kuroshio meander component (Fig. 7, blue line). The standard deviation of this component is 2.97 Sv, larger than both annual variation and mesoscale eddy components. The transport variation related with this component (Fig. 6b, blue line) has a smaller magnitude from May to September compared to the rest.

5. Discussion

5.1. Transport through Kerama Gap in relation to transport through Miyakojima to Okinawa and the PN line

Kerama Gap has been suggested as a key region for interaction between the ECS-Kuroshio and the Ryukyu Current (Nitani 1972; Andres et al. 2008a, b; Jin et al. 2010), but the deep gap's width (∼50 km) is much less than the total distance from Miyakojima to Okinawa (∼250 km). The HYCOM 20-year reanalysis provides an opportunity to compare the mean transport through the smaller passage (Kerama
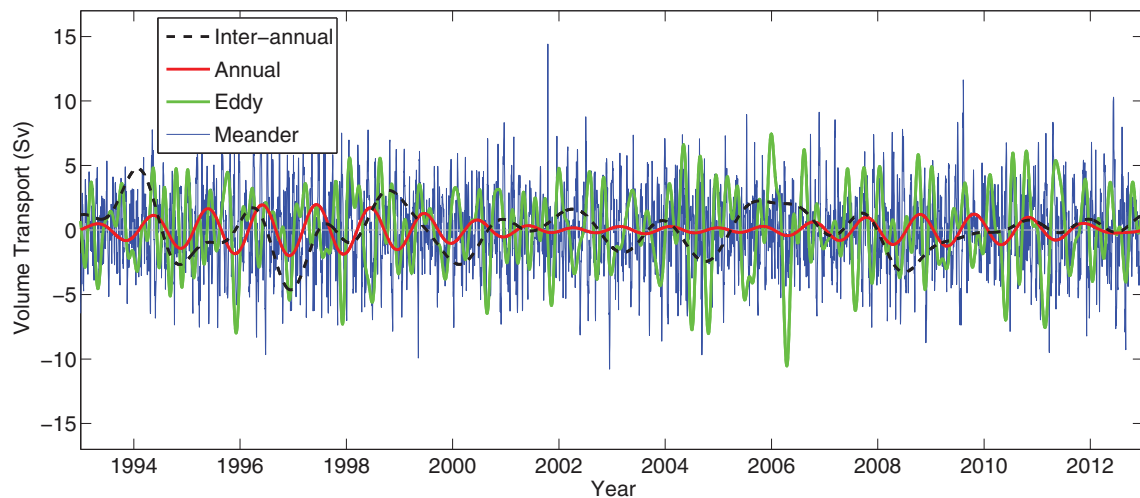
Fig. 7. The transport inter-annual variation component (black dashed line, 20-year mean removed), annual variation component (red), mesoscale eddy component (green), and Kuroshio meander component (blue) from 1993 to 2012 through Kerama Gap from the 1/12.5° global HYCOM reanalysis. (For interpretation of the references to color in this figure legend, the reader is referred to the web version of this article).
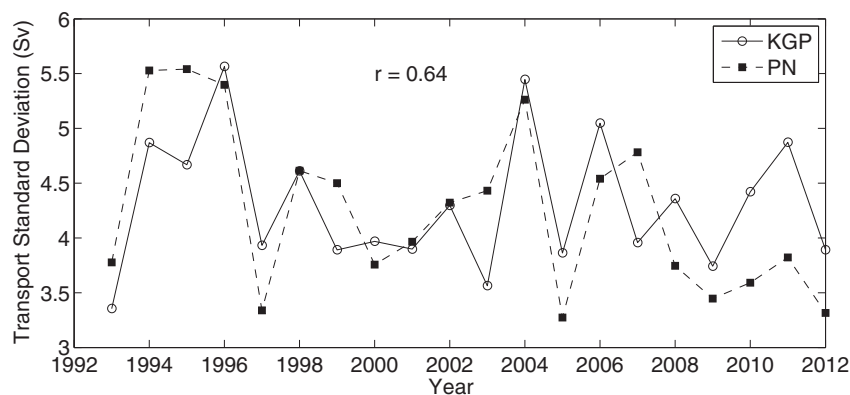

Fig. 8. Comparison of yearly transport standard deviation between transport through Kerama Gap (solid line) and the PN line (dashed line) for 1993–2012 from the 1/12.5° global HYCOM reanalysis.

Gap) and the larger passage (from Miyakojima to Okinawa). Mean transport through the passage between Miyakojima and Okinawa is 2.03 Sv into ECS, with a standard deviation of 5.74 Sv. The mean transport through Kerama Gap represents 96% of the mean transport between Miyakojima and Okinawa. Thus the transport through Kerama Gap is confirmed to be a good approximation to the mean transport between Miyakojima and Okinawa, as mentioned earlier in Section 1.

To confirm the conclusions derived from observations that Kerama Gap transport may have a significant impact on the temporal variability of the Kuroshio transport in the ECS, we calculate the standard deviation of the transport through Kerama Gap and the PN line every year. The two time series of standard deviation are highly correlated with a correlation coefficient of 0.64 (Fig. 8), confirming that the temporal variability of the Kuroshio transport in the ECS (PN line) corresponds well with the transport variation through Kerama Gap.

5.2. Transport in year-1 vs. year-2

In this section, we explain a possible mechanism underlying the 1.0 Sv inflow increase from year-1 (1.6 Sv) to year-2 (2.6 Sv) in the HYCOM reanalysis. The yearly averaged inter-annual variation component (black dashed line in Fig. 7 in which the 1.95 Sv mean transport is removed) is 0.3 Sv in year-2 and -0.3 Sv in year-1, and thus explains the transport increase of 0.6 Sv from year-1 to year-2. The 2-year average inter-annual signal is zero, which helps to explain why the 2-year mean transport is almost the same as the 20-year mean. Cummings

and Smedstad (2013) have already verified that the assimilated SSH field in the Kuroshio region shows good agreement with independent infrared frontal analyses performed by the Naval Oceanographic Office. Thus we treat the assimilated SSH as the "true" state. The yearly averaged SSH difference, defined as SSH in year-2 minus in year-1, shows an anomalous cyclone to the south-southeast of Kerama Gap (Fig. 9) with an SSH difference across the HYCOM Kerama Gap transect of 1.1 cm. The correlation coefficient between the SSH difference across the HYCOM Kerama Gap transect and the transport through Kerama Gap is 0.83 over the 20-year reanalysis period. The regression coefficient between the SSH difference across the HYCOM Kerama Gap transect and transport is 0.46 Sv/cm. Thus the SSH difference between year-2 and year-1 explains 0.5 Sv of the transport difference. This indicates that the difference between yearly averaged transport in year-1 and year-2 corresponds well with the difference between yearly averaged SSH differences in year-1 and year-2. It can be concluded that about one half of the increase of yearly averaged inflow from year-1 to year-2 can be attributed to the increase of yearly averaged inter-annual variation component of inflow transport which is accompanied with the development of an anomalous cyclonic eddy to the south-southeast of Kerama Gap from year-1 to year-2.

5.3. Ekman dynamics

The dynamics underlying the annual variation component are attributed to the wind-driven Ekman transport. The mean winds over
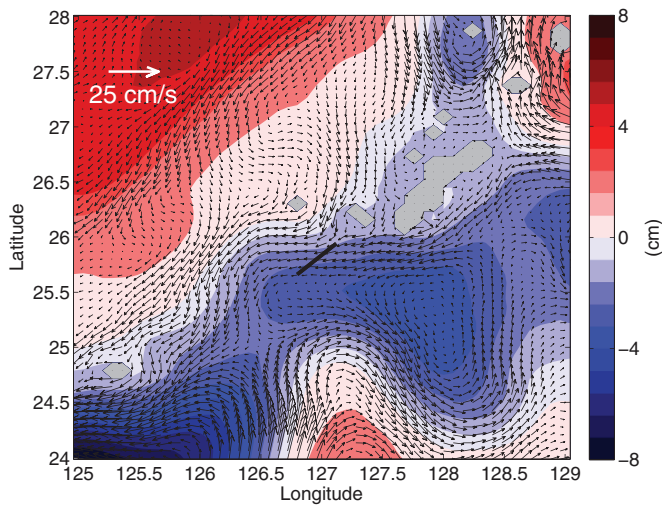
Fig. 9. SSH difference (year-2–year-1, cm) and layer-1 velocity difference (year-2–year-1, cm/s) between year-2 (June 2010–June 2011) and year-1 (June 2009–June 2010) from the global HYCOM reanalysis.

the broad shelf of the ECS are dominated by the East Asia monsoon. In summer (June–August), the wind is north–northwestward at Kerama Gap (Fig. 10a), while in the winter (December–February) the wind is southwestward and stronger (Fig. 10b). With the prevailing seasonal wind blowing toward the northwest (southwest) persistently in summer (winter), water piles up on the northeast (northwest) flank of Kerama Gap due to Ekman transport. Thus the corresponding geostrophic flow is northwestward (southwestward), parallel to the wind direction and causes the water to flow into (out of) the ECS through Kerama Gap. The annual variation component of area-averaged (between 126.0° and 127.5°E, 25.4° and 26.7°N) monthly along Kerama Gap wind stress anomaly (30° counter-clockwise from north) shows good agreement with the monthly transport of the annual variation component (Fig. 10c) and the correlation coefficient is 0.55. Hsin et al. (2010) found a similar relationship near southeastern Taiwan, where the geostrophic velocity and local meridional wind stress are generally well-correlated on the seasonal time scale.

5.4. Monthly mean SSH anomaly

Unlike Na et al. (2014), the mesoscale eddy component is represented by a group of peaks with similar amplitude (Fig. 5) in the

period band 70–200 days, instead of a single dominant peak at ∼100-day period. The period band 70–200 days agrees well with the dominant time scale of the transport mode through the ETC reported by Zhang et al. (2001). Spectral analysis using the reanalysis transport time series from only the 2-year observational period does show a single dominant peak at ∼100-day period, the same as observations. This indicates that time intervals of arriving mesoscale eddies from the interior ocean vary with time over the 20-year period, and are not dominated by a single 100-day time period.

In order to explain the monthly mean of the mesoscale eddy component (green line in Fig. 6b), we generated a monthly mean SSH anomaly (SSHA) map centered on Kerama Gap (Fig. 11). An EOF analysis was performed and the leading mode of the annual steric effect (Stammer, 1997) was also removed. Depending on the eddy location, the same type of eddy can increase or decrease transport through Kerama Gap. The mesoscale eddies typically propagate into this region as part of the return flow of the Kuroshio's non-linear recirculation gyre. Therefore, it can be concluded that the Kuroshio's non-linear recirculation gyre is one of the possible reasons for the significant month to month variations shown in Fig. 11. Andres et al. (2008a) show that positive transport anomalies in Kerama Gap are associated with the arrival of anticyclonic eddies along the eastern side of Okinawa, while negative transport anomalies are associated with the arrival of cyclonic eddies. Na et al. (2014) find that cyclonic (anticyclonic) eddies increase (decrease) transport through Kerama Gap when these eddies are located to the south of Kerama Gap.

Below, we examine the reason why the contributions of eddies to the transport seasonal cycle are large in January–May and October–December (Fig. 6b, green line), and small from June to September. During the inflow stage, an anomalous anticyclone is located to the east of Okinawa in January and to the southeast of Kerama Gap in February. A dipole with an anticyclone (cyclone) attached to the northern (southern) Kerama Gap is shown in October. When both eddies pump water into ECS through Kerama Gap, the maximum inflow occurs in October. But the SSHA map in May shows an exception. When a cyclone is located to the east of Okinawa in May, the eddy should decrease transport (Andres et al., 2008a) instead of increasing transport (Fig. 6b, green line).

A cyclonic eddy located to the east of Okinawa and an anticyclonic eddy to the south/southeast of Kerama Gap is consistent with outflow from the ECS through Kerama Gap, as occurs in March and April. But during November and December, an elongated anticyclonic eddy that straddles the entire passage from Miyakojima to Okinawa separates two cyclones located to the southeast and northwest of Kerama Gap. The anticyclone straddling Kerama Gap would
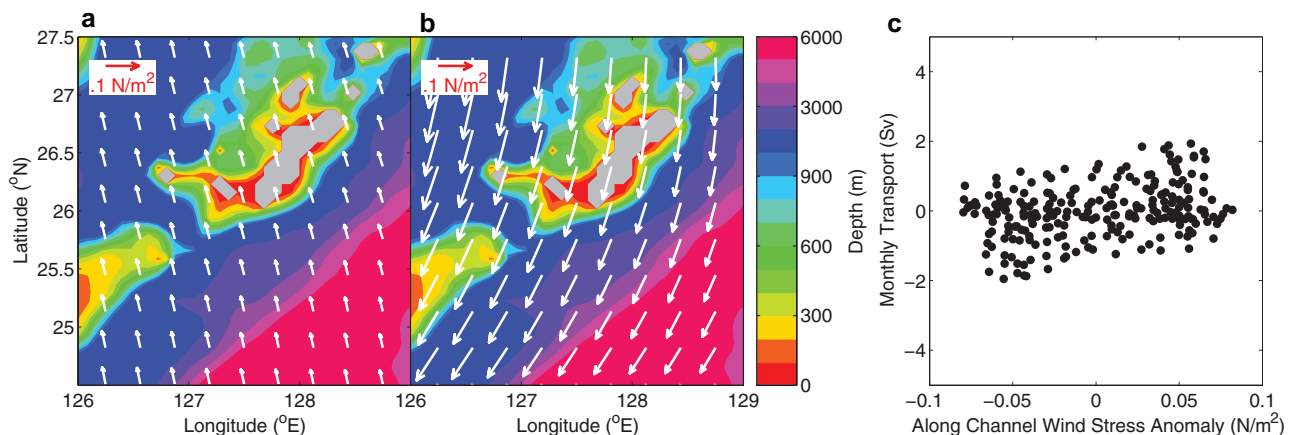

Fig. 10. Mean CFSR wind stress vectors averaged over the period 1993–2012 in the ECS during summer (a, June–August) and winter (b, December–February). Gray represents model land points. The reference vector is shown in the upper left corner of each panel. (c) Scatter plot of annual variation component of monthly along Kerama Gap wind stress anomaly (N/m²) and monthly transport (Sv) of the annual variation component through Kerama Gap.
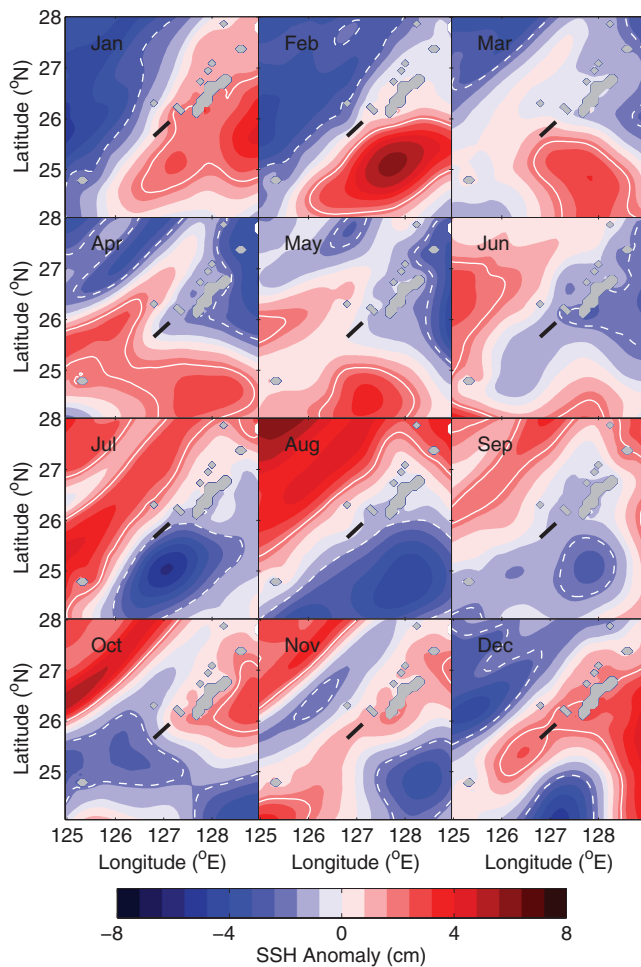
Fig. 11. Monthly mean (1993–2012) SSHA (cm, relative to annual mean SSH with annual steric effect removed) pattern from January to December. Contours with SSHA = 2 cm (solid white line) are used to identify the anomalous anticyclones and contours with SSHA = −2 cm (dashed white lines) are used to identify the anomalous cyclones.

suggest weak flow instead of the strong outflow shown by the monthly mean.

The vertical structure of the normal velocity anomaly in May (November and December) shows that subsurface water primarily flows into (out of) the ECS through Kerama Gap. Jin et al. (2010)

applied the self-organizing map to study the interaction between the ECS and the Ryukyu Current through Kerama Gap. Four coherent patterns were extracted to illustrate how eddies in the ECS interact with eddies in the Ryukyu Current to alter the flow through Kerama Gap. The velocity anomaly structure in May (Fig. 12a) and November (Fig. 12b) belongs to patterns P4 and P3 (Fig. 2d and c in Jin et al., 2010, respectively). Thus the transport anomaly in May, November, and December (velocity anomaly structure in December is very similar to November and is not shown) is caused by eddy interactions on the western and eastern sides of Kerama Gap and is associated with deeper levels, but is not represented by the SSHA.

Small eddy contributions to the transport seasonal cycle from June to September indicate that the impact of eddies on the transport through Kerama Gap is small during these four months and the SSHA maps confirm this. The cyclonic eddies are either far away from Kerama Gap (June and September) or oriented along the Kerama Gap transect and thus generate small SSH difference across the transect (July and August) (and additionally have negligible deep flow).

5.5. Baroclinic instability

Previous studies have shown that baroclinic instabilities lead to Kuroshio meander variations (James et al., 1999; Zhang et al., 2001; Nakamura et al., 2003; Hsin et al., 2008). Charney (1947) developed the baroclinic instability theory for large scale quasi-geostrophic atmospheric waves while Orlanski and Cox (1973) show us how baroclinic instability develops when horizontal density gradients are present in the ocean. The horizontal density/temperature gradient is essential since it provides the available potential energy for the growth of the baroclinic instability. The horizontal temperature gradient between Kuroshio water and the ambient ECS water shows a seasonal cycle: weak in summer and strong during the winter-spring period (Nagata and Takeshita, 1985). Thus, the baroclinic instability is suppressed (enhanced) in summer (winter and spring) as shown in Fig. 6b (blue line). Previous observations (Nakamura et al., 2006, 2008) have indicated that the Kuroshio pathway in the northern Okinawa Trough is destabilized during the winter–spring period and stabilized during the summer–autumn period. Nakamura et al. (2010, 2012) additionally examined this seasonality of the Kuroshio pathway destabilization and found that baroclinic instability triggered by nonlinear Ekman divergence due to wind stress in autumn and winter plays an important role in Kuroshio pathway variation. Thus the observed transport variability seems to be explained by the theoretical considerations on the internal baroclinic instability.
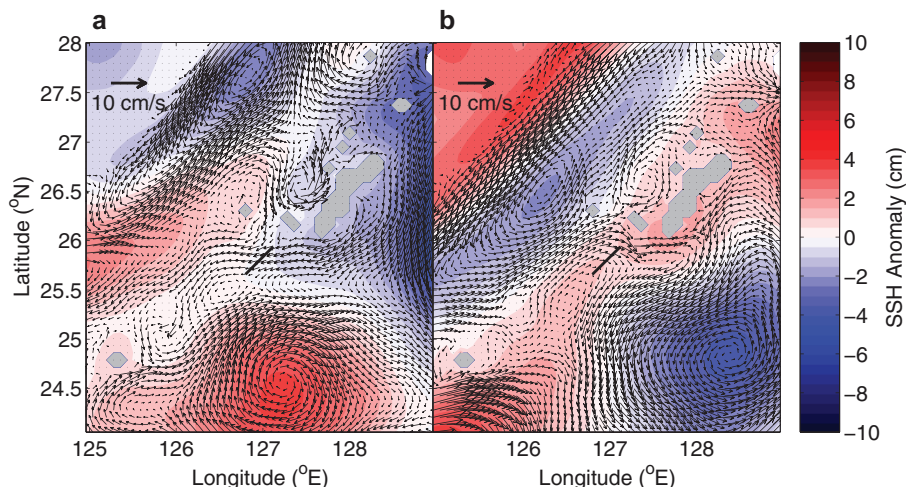

Fig. 12. Monthly velocity anomaly (cm/s, relative to annual mean velocity) at 150 m overlaid on top of the SSHA in May (a) and November (b). The reference vector is shown in the upper left corner of each panel.

6. Conclusions

A global HYCOM data-assimilative reanalysis was integrated for 20 years from 1993 to 2012 and used to study the transport variability through Kerama Gap, the deepest channel in the Ryukyu Islands Arc, and an important passage for water exchange between the ECS and the Northwest Pacific. The reanalysis volume transport time series through Kerama Gap was confirmed to accurately reproduce the 2-year observational time series from June 2009 to June 2011 reported by Na et al. (2014). The discrepancy of the bottom velocity between the reanalysis and observations confirms that MODAS has marginal skill in areas where profiles are limited. From the 20-year transport time series of volume transport, we estimated the 20-year monthly mean seasonal cycle that has the maximum in October (3.0 Sv) and the minimum in November (0.5 Sv).

The transport time series has large variability with a maximum of 17.3 Sv (May 1994) and minimum of −14.5 Sv (December 1996). The 20-year mean of the volume transport is 1.95 Sv into the ECS. Its standard deviation is 4.0 Sv, equal to the observed standard deviation of the ECS Kuroshio volume transport at the PN-line (Andres et al., 2008b), which indicates a significant impact of Kerama Gap transport on the temporal variability of the Kuroshio transport in the ECS.

The annual variation component, with periods between 345 and 400 days, explains only 2.3% of the total transport variance, but it makes a significant contribution to the seasonal cycle (Fig. 6b, red line). This variation component tends to accompany an increase of inflow through Kerama Gap in summer and a decrease in winter. It is explained by the Ekman dynamics responding to seasonal changes of the local winds, which contribute a positive transport anomaly in summer and a negative transport anomaly in winter.

The mesoscale eddy component, with periods between 70 and 345 days, makes the most significant contribution to the transport seasonal cycle except during summer from June to September (Fig. 6b, green line). The impinging mesoscale eddies substantially affect the monthly mean, increase the transport into the ECS during January, February, May, and October, and decrease it in March, April, November, and December. In summer, contributions of impinging cyclonic and anticyclonic eddies are nearly equal to each other, and the apparent influence of eddies diminishes.

The contribution of the Kuroshio meander components with periods shorter than 70 days to the seasonal cycle is larger in winter than in summer. Baroclinic instability was suggested to be one possible explanation.

The contribution of the inter-annual component to the seasonal cycle is just the 20-year mean transport (Fig. 6a, black dashed line) due to its long time period and thus is not discussed in this paper. However, we will present the inter-annual component of the volume transport in a separate paper that examines its impact on extreme flow events, i.e., when transport anomaly exceeds one standard deviation.

References

Andres, M., Park, J.-H., Wimbush, M., Zhu, X.-H., Chang, K.-I., Ichikawa, H., 2008a. Study of the Kuroshio/Ryukyu current system based on satellite-altimeter and in situ measurements. J. Oceanogr. 64, 937–950.

Andres, M., Wimbush, M., Park, J.-H., Chang, K.-I., Lim, B.-H., Watts, D.R., Ichikawa, H., Teague, W.J., 2008b. Observations of Kuroshio flow variations in the East China Sea. J. Geophys. Res. 113, C05013. doi:10.1029/2007JC004200.

Andres, M., Cenedese, C., 2013. Laboratory experiments and observations of cyclonic and anticyclonic eddies impinging on an island. J. Geophys. Res. Oceans 118. doi:10.1002/jgrc.20081.

Bleck, R., 2002. An oceanic general circulation model framed in hybrid isopycnic-Cartesian coordinates. Ocean Modell. 4, 55–88.

Charney, J.G., 1947. The dynamics of long waves in a baroclinic westerly current. J. Meteorol. 4, 135–162.

Chassignet, E.P., Smith, L.T., Halliwell, G.R., Bleck, R., 2003. North Atlantic simulations with the Hybrid Coordinate Ocean Model (HYCOM): impact of the vertical coordinate choice, reference pressure, and thermobaricity. J. Phys. Oceanogr. 33, 2504–2526.

Choi, B.H., Kim, K.O., Eum, H.M., 2002. Digital bathymetric and topographic data for neighboring seas of Korea. J. Korean Soc. Coast. Ocean Eng. 14, 41–50.

Cummings, J.A., 2005. Operational multivariate ocean data assimilation. Q. J. R. Meteorol. Soc. 131, 3583–3604.

Cummings, J.A., Smedstad, O.M., 2013. Variational data assimilation for the global ocean. In: Park, S.K., Xu, L. (Eds.). Data Assimilation for Atmospheric, Oceanic, and Hydrologic Applications (Vol. II). Springer-Verlag, Berlin, Heidelberg http://dx.doi.org/10.1007/978-3-642-35088-7_13 .

Dewar, W.K., Bane, J.M., 1985. Subsurface energetics of the Gulf Stream near the Charleston Bump. J. Phys. Oceanogr. 15, 1771–1789.

Feng, M., Mitsudera, H., Yoshikawa, Y., 2000. Structure and variability of the Kuroshio current in Tokara Strait. J. Phys. Oceanogr. 30, 2257–2276.

Fox, D.N., Teague, W.J., Barron, C.N., Carnes, M.R., Lee, C.M., 2002. The modular ocean data assimilation system. J. Atmos. Ocean. Technol. 19, 240–252.

Gordon, A.L., Flament, P., Villanoy, C., Centurioni, L., 2014. The nascent Kuroshio of Lamon Bay. J. Geophys. Res. Oceans 119, 4251–4263. doi:10.1002/2014JC009882.

Guo, X., Miyazawa, Y., Yamagata, T., 2006. The Kuroshio onshore intrusion along the shelf break of the East China Sea: the origin of the Tsushima warm current. J. Phys. Oceanogr. 36, 2205–2231.

Helber, R.W., T.L. Townsend, C.N. Barron, J.M. Dastugue, and M.R. Carnes, 2013. Validation Test Report for the Improved Synthetic Ocean Profile (ISOP) System: Part I. Synthetic Profile Methods and Algorithm. NRL memorandum report NRL/MR/7320–13-9364, http://www7320.nrlssc.navy.mil/pubs/2013/helber1-2013.pdf.

Hsin, Y.-C., Wu, C.-R., Shaw, P.-T., 2008. Spatial and temporal variations of the Kuroshio east of Taiwan, 1982–2005: a numerical study. J. Geophys. Res. 113, C04002. doi:10.1029/2007JC004485.

Hsin, Y.-C., Qu, T., Wu, C.-R., 2010. Intra-seasonal variation of the Kuroshio southeast of Taiwan and its possible forcing mechanism. Ocean Dyn. 60, 1293–1306.

Ichikawa, H., Nakamura, H., Nishina, A., Higashi, M., 2004. Variability of north-eastward current southeast of northern Ryukyu Islands. J. Oceanogr. 60, 351–363.

Ichikawa, K., 2001. Variation of the Kuroshio in the Tokara Strait induced by meso-scale eddies. J. Oceanogr. 57, 55–68.

James, C., Wimbush, M., Ichikawa, H., 1999. Kuroshio meanders in the East China Sea. J. Phys. Oceanogr. 29, 259–272.

Jin, B., Wang, G., Liu, Y., Zhang, R., 2010. Interaction between the East China Sea Kuroshio and the Ryukyu Current as revealed by the self-organizing map. J. Geophys. Res. 115, C12047. doi:10.1029/2010JC006437.

Johns, W.E., Lee, T.N., Zhang, D., Zantopp, R., Liu, C.-T., Yang, Y., 2001. The Kuroshio east of Taiwan: moored transport observations from the WOCE PCM-1 array. J. Phys. Oceanogr. 31, 1031–1053.

Kundu, P.K., Cohen, I.M., 2002. Fluid Mechanics. Academic Press, San Diego.

Lee, I.-H., Ko, D.S., Wang, Y.-H., Centurioni, L., Wang, D.-P., 2013. The mesoscale eddies and Kuroshio transport in the western North Pacific east of Taiwan from 8-year (2003–2010) model reanalysis. Ocean Dyn. 63, 1027–1040.

Metzger, E.J., Smedstad, O.M., Thoppil, P.G., Hurlburt, H.E., Cummings, J.A., Wallcraft, A.J., Zamudio, L., Franklin, D.S., Posey, P.G., Phelps, M.W., Hogan, P.J., Bub, F.L., Dehaan, C.J., 2014. US Navy operational global Ocean and Arctic ice prediction systems. Oceanography 27, 32–43.

Morinaga, K., Nakagawa, N., Osamu, K., Guo, B., 1998. Flow pattern of the Kuroshio west of the main Okinawa Island. In: Proceedings of Japan–China Joint Symposium on Cooperative Study of Subtropical Circulation System. Seikai National Fisheries Research Institute, Nagasaki, Japan, pp. 203–210.

Na, H., Wimbush, M., Park, J.-H., Nakamura, H., Nishina, A., 2014. Observations of flow variability through the Kerama Gap between the East China Sea and the northwestern Pacific. J. Geophys. Res., Oceans 119, 689–703. doi:10.1002/2013JC008899.

Nagata, U., Takeshita, K., 1985. Variation of the sea surface temperature distribution across the Kuroshio in the Tokara Strait. J. Oceanogr. Soc. Jpn. 41, 244–258.

Nakamura, H., Ichikawa, H., Nishina, A., Lie, H.-J., 2003. Kuroshio path meander between the continental slope and the Tokara Strait in the East China Sea. J. Geophys. Res. 108 (C11), 3360. doi:10.1029/2002JC001450.

Nakamura, H., Nishina, A., Ichikawa, H., 2006. Time-frequency variability of Kuroshio meanders in Tokara Strait. Geophys. Res. Lett. 33, L21605. doi:10.1029/2006GL027516.

Nakamura, H., Nishina, A., Ichikawa, H., Nonaka, M., Sasaki, H, 2008. Deep countercurrent beneath the Kuroshio in the Okinawa trough. J. Geophys. Res. 113, C06030. doi:10.1029/2007JC004574.

Nakamura, H., Nonaka, M., Sasaki, H., 2010. Seasonality of the Kuroshio path destabilization phenomenon in the Okinawa Trough: a numerical study of its mechanism. J. Phys. Oceanogr. 40, 530–550. doi:10.1175/2009JPO4156.1.

Nakamura, H., Nishina, A., Tabata, K., Higashi, M., Habano, A., Yamashiro, T., 2012. Surface velocity time series derived from satellite altimetry data in a section across the Kuroshio southwest of Kyushu. J. Oceanogr. 68, 321–336. doi:10.1007/s10872-012-0101-4.

Nakamura, H., Nishina, A., Liu, Z., Tanaka, F., Wimbush, M., Park, J.-H., 2013. Intermediate and deep water formation in the Okinawa Trough. J. Geophys. Res. 118, 6881–6893.

Nitani, H., 1972. Beginning of the Kuroshio. Kuroshio. University of Washington Press, Seattle, pp. 129–163.

Oka, E., Kawabe, M., 1998. Characteristics of variations of water properties and density structure around the Kuroshio in the East China Sea. J. Oceanogr. 54, 605–617.

Orlanski, I., Cox, M., 1973. Baroclinic instability in ocean currents. Geophys. Fluid Dyn. 4, 297–332.

Qiu, B., 2001. Kuroshio and Oyashio Currents. Encyclopedia of Ocean Sciences, 3. Academic Press, San Diego, CA, pp. 1413–1425.

Qiu, B., Toda, T., Imasato, N., 1990. On Kuroshio front fluctuations in the East China Sea using satellite and in situ observational data. J. Geophys. Res. 95, 18191–18204.

Qu, T., Lukas, R., 2003. The bifurcation of the North Equatorial Current in the Pacific. J. Phys. Oceanogr. 33, 5–18.

Roemmich, D., McCallister, T., 1989. Large scale circulation of the North Pacific Ocean. Prog. Oceanogr. 22, 171–204.

Saha, S., others, 2010. The NCEP climate forecast system reanalysis. Bull. Am. Meteorol. Soc. 91, 1015–1057 http://dx.doi.org/10.1175/2010BAMS3001.1 .

Soeyanto, E., Guo, X., Ono, J., Miyazawa, Y., 2014. Interannual variations of Kuroshio transport in the East China Sea and its relation to the Pacific decadal oscillation and mesoscale eddies. J. Geophys. Res. Oceans 119, 3595–3616. doi:10.1002/2013JC009529.

Sugimoto, T., Kimura, S., Miyaji, K., 1988. Meander of the Kuroshio front and current variability in the East China Sea. J. Oceanogr. Soc. Jpn. 44, 125–135.

Stammer, D., 1997. Steric and wind-induced changes in TOPEX/POSEDON large-scale sea surface topography observations. J. Geophys. Res. 102, 20,987–21,009.

Thoppil, P., Metzger, E.J., Hurlburt, H.E., Smedstad, O.M., Ichikawa, H., 2015. The current system east of the Ryukyu Islands as revealed by a global ocean reanalysis. Submitted to Prog. Oceanogr 751–753.

You, S.-H., Yoon, J.-H., 2004. Modeling of the Ryukyu current along the Pacific side of the Ryukyu Islands. Pacific Oceanogr. 2, 44–51.

Yuan, Y., Takano, K., Pan, Z., Su, J., Kawatate, K., Imawaki, S., Yu, H., Chen, H., Ichikawa, H., Umatani, S., 1994. The Kuroshio in the East China Sea and the currents east of the Ryukyu Islands. La Mer 32, 235–244.

Yuan, Y., Su, J., Pan, Z., Chen, H., Ichikawa, H., Imawaki, S., Kawatate, K., Takano, K., Umatani, S.-I., 1995. The western boundary current east of the Ryukyu Islands. La Mer 33, 1–11.

Zhang, D., Johns, W.E., Lee, T.N., Liu, C.-T., Zantopp, R., 2001. The Kuroshio east of Taiwan: modes of variability and relationship to interior mesoscale eddies. J. Phys. Oceanogr. 31, 1054–1074.